(Polymer Program) and by the donors of the Petroleum Research Fund, administered by the American Chemical Society. S.S. is grateful to the American Association of University Women (AAUW) for the 1991/1992 Founders' Fellowship. We thank Du Pont and Dow Companies for the gift of the perfluorinated membranes and the reviewers for their helpful comments and criticism.

Registry No. MV^{2+}, 1910-42-5; $Ru(bpy)_3^{2+}$, 15158-62-0; O_2, 7782-44-7; H_2O, 7732-18-5; MeOH, 67-56-1; EtOH, 64-17-5; Nafion 117, 66796-30-3.

Preparation, Characterization, and Ionic Conductivity of Novel Crystalline, Microporous Germanates, $M_3HGe_7O_{16}{\cdot}xH_2O$, M = NH_4^+, Li^+, K^+, Rb^+, Cs^+; x = 4–6. 2

Shouhua Feng and Martha Greenblatt*

Department of Chemistry, Rutgers, The State University of New Jersey, Piscataway, New Jersey 08855-0939

Received November 20, 1991. Revised Manuscript Received January 14, 1992

A series of crystalline, microporous germanates, $M_3HGe_7O_{16}{\cdot}xH_2O$, M = NH_4^+, Li^+, x = 6; M = K^+, Rb^+, Cs^+, x = 4, were synthesized hydrothermally and characterized by powder X-ray diffraction, differential thermal analysis, and thermogravimetric analysis. Ionic conductivity in both hydrated and dehydrated samples was investigated by ac impedance in the temperature range 25–550 °C. The protonic conductivity is highest in $(NH_4)_3HGe_7O_{16}{\cdot}6H_2O$, 3.1×10^{-4} $(\Omega\ cm)^{-1}$ at 144 °C. The best ionic conductivity was found in $Cs_3HGe_7O_{16}$, 2.0×10^{-3} $(\Omega\ cm)^{-1}$ at 400 °C. The ionic conductivity of dehydrated $M_3HGe_7O_{16}$ increases and the activation energy decreases with increasing cation radius from room temperature to 500 °C. This behavior is consistent with a reduced Coulombic attraction between the mixed tetrahedral–octahedral (GeO_4–GeO_6) anion framework structure of the germanates and the cations located in their channels, compared with that in other zeolite-type compounds.

1. Introduction

Crystalline microporous materials are widely used in the fields of catalysis, ion exchange, and adsorption.[1-3] There have been many attempts to develop and improve electrical conductivity in the crystalline microporous materials, which contain open channels on the molecular scale and exchangeable cations; the channels serve as conducting paths for the mobile ions. Ionic conductivity studies in a number of aluminosilicate zeolites have been made, with special focus on the ion-exchange properties of zeolite samples and on the effect of different channel dimensions (i.e., aperture size) on the ionic conductivity.[4-10] However, the ionic conductivity in these materials is low compared to known fast ionic conductors. The reasons for the low conductivity in zeolitic materials are 2-fold: (1) the negatively charged framework structure of traditional zeolites has very strong attraction for cations, which hinders ion migration;[11] (2) the size of channels or cages in some of the zeolites is so large that the mobile ions are trapped on the walls of the channels or cages. Thus decreasing the electrostatic interaction between the anion framework structure and the cations and matching the ion-channel size are important factors in improving ionic conductivity of zeolitic materials. To investigate these effects, we have chosen a novel crystalline microporous sodium hydrogen germanate, $Na_3HGe_7O_{16}{\cdot}xH_2O$, with a mixed, tetrahedral–octahedral framework structure closely related to zeolitic materials.[12-20] Previous studies on $Na_3HGe_7O_{16}{\cdot}xH_2O$ showed protonic conductivity $\sim10^{-4}$ $(\Omega\ cm)^{-1}$ at 50 °C and sodium ionic conductivity $\sim10^{-3}$ $(\Omega\ cm)^{-1}$ at 500 °C on dehydrated samples.[21] We have continued to investigate ionic conductivity in this structure with other ions, in order to understand the mechanism of ionic conduction and to search for fast ionic conductors in zeolite-like materials. The crystalline microporous germanates, $M_3HGe_7O_{16}{\cdot}4$–

* To whom correspondence should be addressed.

(1) Barrer, R. M. *Hydrothermal Chemistry of Zeolites*; Academic Press: London, 1982.
(2) Rabo, J. A., Ed. *Zeolite Chemistry and Catalysis*; American Chemical Society: Washington, DC, 1976.
(3) Flank, W. H., Ed. *Adsorption and Ion Exchange with Synthetic Zeolites, Principle and Practice*; ACS Symposium Series 135; American Chemical Society: Washington, DC, 1980.
(4) Breck, D. W. *Zeolite Molecular Sieves, Synthesis, Structure and Use*; Wiley: London, 1974; p 457.
(5) Schoonheydt, R. A.; Velghe, F. *J. Chem. Soc., Faraday Trans* **1976**, *72*, 172.
(6) Schoonheydt, R. A. *Proceedings of 5th International Zeolite Conference*; Rees, L. V. C., Ed.; Heyden: London, 1980; p 242.
(7) Kelemen, G.; Lortz, W.; Schon, G. *J. Mater. Sci.* **1989**, *24*, 333.
(8) Kreuer, K. D.; Weppner, W.; Rabenan, A. *Mater. Res. Bull.* **1982**, *17*, 501.
(9) Andersen, E. K.; Andersen, I. G. K.; Skou, E.; Yde-Andersen, S. *Solid State Ionics* **1986**, *18, 19*, 1170.
(10) Welletr, M. T.; Dodd, S. M.; Jiang, M. R. M. *J. Mater. Chem.* **1991**, *1*, 11.
(11) West, A.R. *Solid State Chemistry and Its Applications*; Wiley: New York, 1984; p 452.
(12) Corcoran, E. W., Jr.; Nawsam, J. M.; King, H. E., Jr.; Vaughan, D. E. W. *Zeolite Synthesis*; Occelli, M., Robson, H. E., Eds.; American Chemical Society: Washington, DC, 1989; p 603.
(13) Feng, S.; Xu, R.; Yang, G.; Shun, H. *Chem. J. Chinese Univ. (Engl. Ed.)* **1988**, *4*, 9.
(14) Wang, T.; Yang, G.; Feng, S.; Shang, C.; Xu, R. *J. Chem. Soc., Chem. Commun.* **1989**, 2436.
(15) Zemann, V. J. *Acta Crystallogr.* **1959**, *12*, 252.
(16) H. Bittner, H.; Kerber, W. *Monatsh. Chem.* **1969**, *100*, 427.
(17) Hauser, E.; Nowotny, H.; Seifert, K. J. *Monatsh. Chem.* **1970**, *101*, 715.
(18) Hauser, E.; Bittner, H.; Nowotny, H. *Monatsh. Chem.* **1970**, *101*, 1864.
(19) Hauser, E.; Hoch, M. J. R. *J. Magn. Reson.* **1973**, *10*, 211.
(20) Nowotny, H.; Wittmann, A. *Monatsh. Chem.* **1954**, *85*, 558.
(21) Feng, S.; Tsai, M.; Greenblatt, M. *Chem. Mater.*, in press.

0897-4756/92/2804-0462$03.00/0

Table I. Hydrothermal Synthetic Conditions for $M_3HGe_7O_{16}\cdot 4\text{-}6H_2O$, M = NH_4^+, K^+, Rb^+, and Cs^+

	$xM_2O\cdot yGeO_2\cdot zH_2O$			crystallization		
run no.	x	y	z	temp, °C	time, h	crystalline product
SN202	1.5	1.0	150	180	72	$(NH_4)_3HGe_7O_{16}\cdot 6H_2O$
SK202	1.0	1.0	100	180	48	$K_3HGe_7O_{16}\cdot 4H_2O$
SR202	1.0	1.0	120	180	48	$Rb_3HGe_7O_{16}\cdot 4H_2O$
SC202	0.8	1.0	120	180	72	$Cs_3HGe_7O_{16}\cdot 4H_2O$

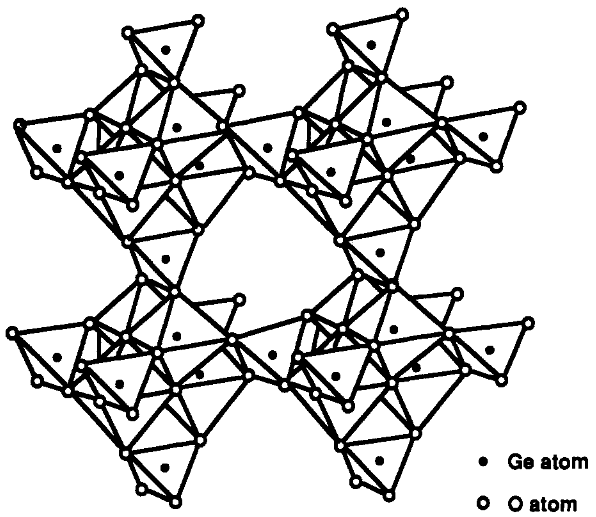

Figure 1. Framework structure of the germanate showing the linkage of GeO_4 tetrahedra and GeO_6 octahedra.

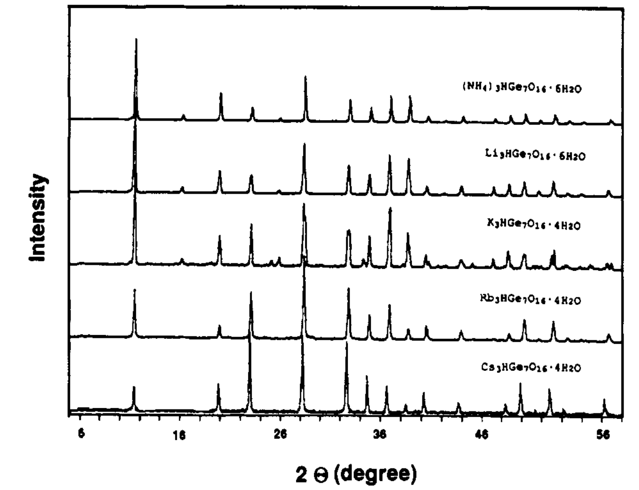

Figure 2. Powder X-ray diffraction patterns for $M_3HGe_7O_{16}\cdot xH_2O$, for M = K^+, Rb^+, and Cs^+, x = 4; M = NH_4^+ and Li^+, x = 6.

$6H_2O$, M = NH_4^+, Li^+, K^+, Rb^+, and Cs^+, are isostructural with $Na_3HGe_7O_{16}\cdot 6H_2O$, which is related to the mineral pharmacosiderite ($KFe_4(AsO_4)_3(OH)_4\cdot 6\text{-}8H_2O$).[22] In the cubic framework structure of the germanates (Figure 1), the basic building units are GeO_6 octahedra and GeO_4 tetrahedra. In contrast, in the aluminosilicate zeolites only TO_4 (T = Si and Al) tetrahedra serve as the basic building units. In the germanate, parts of the framework oxygens (1/4) are four-coordinated with three Ge atoms and one hydrogen atom, which leads to a smaller effective negative charge on the framework. Channels of eight-membered rings with a window size of 4.3 Å lie in the (100) directions where cations and water molecules are located.

In this paper we report results of hydrothermal crystallization, structural characterization, and ionic conductivity of $M_3HGe_7O_{16}\cdot xH_2O$, M = NH_4^+, Li^+, K^+, Rb^+, and Cs^+.

2. Experimental Section

$M_3HGe_7O_{16}\cdot xH_2O$, M = NH_4^+, Na^+, K^+, Rb^+, or Cs^+ was hydrothermally synthesized at 180 °C in a sealed system containing an aqueous mixture of M hydroxide and the α-quartz form of germanium dioxide. A typical synthetic procedure began with the combination of GeO_2 (Eagle-Picher Co., reagent grade) and an aqueous solution of MOH (Fisher, reagent grade) to form an aqueous gel having molar composition $xM_2O\cdot yGeO_2\cdot zH_2O$, where x = 0.5–1.5, y = 1.0, and z = 50–150. Crystallization of the gel was carried out in a stainless steel autoclave lined with poly(tetrafluoroethylene) (PTFE) under autogenous pressure at 180 °C for at least 48 h. The crystalline product was filtered, washed with distilled water, and dried at ambient temperature. $Li_3HGe_7O_{16}\cdot 6H_2O$ was prepared by ion-exchange of $Na_3HGe_7O_{16}\cdot 6H_2O$ in 2 M LiCl solution. The suspension was heated at 80 °C and stirred for 8 h. This procedure was repeated three times. Nearly complete ion exchange (>99%), as determined by chemical analysis, was achieved under the experimental conditions.

Products were characterized by powder X-ray diffraction (XRD) patterns, which were recorded on a Scintag X-ray diffractometer with monochromatized Cu Kα radiation. For the analysis of phase transformation of $Li_3HGe_7O_{16}\cdot 6H_2O$, high-temperature X-ray diffraction was carried out. Unit cell parameters were obtained with a least-squares method with silicon as an internal standard.

(22) Buerger, M. J.; Dollase, W. A.; Garaycochea-Wittke, I. *Z. Kristallogr.* **1967**, *125*, 92.

Table II. Unit Cell Parameters for $M_3HGe_7O_{16}\cdot xH_2O$, M = NH_4^+, Li^+, K^+, Rb^+, and Cs^+

sample	a, Å	V, Å^3
$(NH_4)_3HGe_7O_{16}\cdot 6H_2O$	7.708 (4)	458.0
$Li_3HGe_7O_{16}\cdot 6H_2O$	7.714 (2)	459.0
$K_3HGe_7O_{16}\cdot 4H_2O$	7.720 (0)	460.1
$Rb_3HGe_7O_{16}\cdot 4H_2O$	7.722 (5)	460.5
$Cs_3HGe_7O_{16}\cdot 4H_2O$	7.734 (3)	462.6

Differential thermal and thermogravimetric analysis (DTA and TGA) were carried out on a Du Pont Model 9900 thermal analyzer in air with a heating rate 10 °C/min.

Ionic conductivities were measured by ac impedance technique using a Solartron Model 1250 frequency analyzer and 1186 electrochemical interface that were equipped with a Hewlett-Packard 9816 desktop computer for data collection and analysis. Disk-shaped samples were prepared by a pelletizing pressure of 100 klb/in.^{2}. Electrode connections to the samples were made by coating the faces of the pellets with platinum ink. A frequency range 10 Hz to 65 kHz and a heating rate of 2 °C/min were used throughout. The dehydrated samples were preheated at different temperatures and then cooled in dry Ar prior to ac impedance measurements which were also carried out in flowing dry Ar.

3. Results and Discussion

3.1. Synthesis. Table I lists the starting composition and crystallization conditions for $M_3HGe_7O_{16}\cdot xH_2O$, M = NH_4^+, Na^+, K^+, Rb^+, and Cs^+. $M_3HGe_7O_{16}\cdot xH_2O$ can be crystallized from the starting mixtures with the molar composition range $(0.5\text{-}1.5)M_2O\cdot GeO_2\cdot(50\text{-}150)H_2O$ at 150–180 °C. The MOH content determines the nature and the yield of the desired products. The optimal MOH content necessary to obtain a pure product and good yield was determined empirically. $Li_3HGe_7O_{16}\cdot 6H_2O$ could not be prepared using hydrothermal methods as GeO_2 did not dissolve in an aqueous solution of LiOH, probably due to

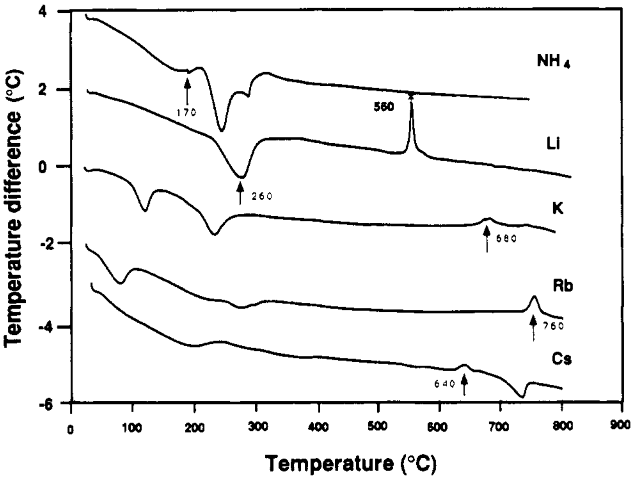

Figure 3. DTA curves for $M_3HGe_7O_{16}{\cdot}4{-}6H_2O$, M = NH_4^+, Li^+, K^+, Rb^+, and Cs^+, showing decomposition temperature. The asterisk represents crystallization temperature.

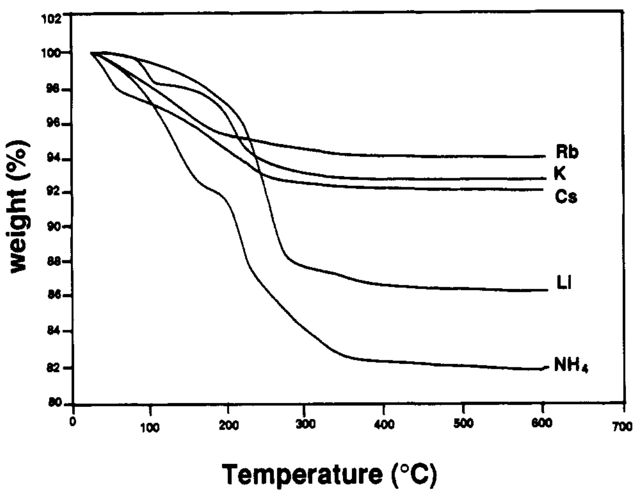

Figure 4. TG curves for $M_3GHe_7O_{16}{\cdot}4{-}6H_2O$, M = NH_4^+, Li^+, Rb^+, and Cs^+.

the low solubility of LiOH which limits the hydroxide ion concentration.

3.2. Structural Characterization. 3.2.1. XRD. Figure 2 shows the XRD patterns of $M_3HGe_7O_{16}{\cdot}xH_2O$ at 25 °C. All of the $M_3HGe_7O_{16}{\cdot}xH_2O$ samples appear to be isostructural. The unit cell parameters (Table II) of $M_3HGe_7O_{16}{\cdot}xH_2O$ were determined by least-squares analysis of the observed PXD data according to the proposed space group $P\bar{4}3m$.[16] From M = NH_4^+ to M = Cs^+ all diffraction peaks gradually shift to lower values of 2θ. This reflects the slight expansion of the volume of the unit cell as the cation radius increases. To identify phases at different level of hydration, both crystalline and amorphous, XRD at variable temperature was used.

3.2.2. DTA and TGA. The DTA (Figure 3) show several endotherms related to water loss in the temperature range 25–350 °C. The order of decomposition or/and phase transformation temperature of $M_3HGe_7O_{16}{\cdot}xH_2O$ is NH_4^+ (170 °C) < Li^+ (260 °C) < Cs^+ (640 °C) < K^+ (680 °C) < Rb^+ (760 °C). It is noteworthy that $Na_3HGe_7O_{16}{\cdot}6H_2O$ has a phase transition to $Na_3HGe_7O_{16}{\cdot}xH_2O$, $x < 4$ at 156 °C, accompanied by loss of $\sim 2H_2O$, but the latter structure is stable up to 556 °C.[21] Thus the order of decomposition temperatures suggests that the Rb^+ ion fits best in the cavities of this structure, while the smaller Li^+ ions and the larger Cs^+ ions destabilize the structure at relatively low temperature. The exotherm of the Li compound in Figure 3 compared with the other germanates is significantly large. This behavior is attributed to phase transformation from an amorphous to a crystalline material in the Li case and decomposition for all the other analogues.

The TG curves (Figure 4) indicate various weight losses corresponding to loss of water (or NH_3). The TG cooling curves (not shown in Figure 4) for M = K^+, Rb^+, and Cs^+ indicate that on cooling, the dehydrated samples adsorb water reversibly at different adsorption rates. The total weight loss of water for $M_3HGe_7O_{16}{\cdot}xH_2O$, M = NH_4^+, Li^+, K^+, Rb^+, and Cs^+ are 12.8, 12.5, 7.2, 7.8, and 6.1%, respectively, corresponding to $x \sim 6$ for M = NH_4^+, Li^+ and $x \sim 4$ for M = K^+, Rb^+, and Cs^+.

On the basis of the DTA-TGA and XRD results, the reactions involved in the thermal processes for $M_3HGe_7O_{16}{\cdot}xH_2O$ can be described as follows:

(1) $(NH_4)_3HGe_7O_{16}{\cdot}6H_2O$

$$(NH_4)_3HGe_7O_{16}{\cdot}6H_2O \rightarrow (NH_4)_3HGe_7O_{16}{\cdot}2H_2 + 4H_2O \quad \text{at 170 °C}$$

$$(NH_4)_3HGe_7O_{16}{\cdot}2H_2O \rightarrow (NH_4)_3HGe_7O_{16}(\text{amorph}) + 2H_2O \quad \text{at 230 °C}$$

(2) $Li_3HGe_7O_{16}{\cdot}6H_2O$

$$Li_3HGe_7O_{16}{\cdot}6H_2O \rightarrow Li_3HGe_7O_{16}{\cdot}5H_2O + H_2O \quad \text{at 200 °C}$$

$$Li_3HGe_7O_{16}{\cdot}5H_2O \rightarrow Li_3HGe_7O_{16}(\text{amorph}) + 5H_2O \quad \text{at 260–550 °C}$$

$$2Li_3HGe_7O_{16}(\text{amorph}) \rightarrow Li_6Ge_8O_{19} + 6GeO_2(\text{amorph}) + H_2O \quad \text{at 560 °C}$$

(3) $K_3HGe_7O_{16}{\cdot}4H_2O$

$$K_3HGe_7O_{16}{\cdot}4H_2O \rightarrow K_3HGe_7O_{16}{\cdot}3H_2O + H_2O \quad \text{at 100 °C}$$

$$K_3HGe_7O_{16}{\cdot}3H_2O \rightarrow K_3HGe_7O_{16} + 3H_2O \quad \text{at 100–400 °C}$$

$$2K_3HGe_7O_{16} \rightarrow 3K_2Ge_4O_9 + 2GeO_2 + H_2O \quad \text{at 680 °C}$$

(4) $Rb_3HGe_7O_{16}{\cdot}4H_2O$

$$Rb_3HGe_7O_{16}{\cdot}4H_2O \rightarrow Rb_3HGe_7O_{16}{\cdot}3H_2O + H_2O \quad \text{at 50 °C}$$

$$Rb_3GHe_7O_{16}{\cdot}3H_2O \rightarrow Rb_3HGe_7O_{16} + 3H_2O \quad \text{at 50–600 °C}$$

$$Rb_3HGe_7O_{16} \rightarrow Rb_4Ge_{11}O_{24} + \text{germanate (unknown)} \quad \text{at 760 °C}$$

(5) $Cs_3HGe_7O_{16}{\cdot}4H_2O$

$$Cs_3HGe_7O_{16}{\cdot}4H_2O \rightarrow Cs_3HGe_7O_{16}{\cdot}H_2O + 3H_2O \quad \text{at 30–180 °C}$$

$$Cs_3HGe_7O_{16}{\cdot}H_2O \rightarrow Cs_3HGe_7O_{16} + H_2O \quad \text{at 180–400 °C}$$

$$2Cs_3HGe_7O_{16} \rightarrow 3Cs_2Ge_4O_9 + 2GeO_2 + H_2O \quad \text{at 640 °C}$$

3.3. Ionic Conductivity. 3.3.1. Hydrated $M_3HGe_7O_{16}{\cdot}xH_2O$. Figure 5 shows the temperature dependence of conductivity of $(NH_4)_3HGe_7O_{16}{\cdot}6H_2O$ and $Li_3HGe_7O_{16}{\cdot}6H_2O$. Due to the phase transformation of the samples at low temperatures, the conductivity of the NH_4^+ and Li^+ analogues was measured below 150 and 200 °C, respectively. The conductivity of samples which were cooled to room temperature and allowed to adsorb water follows the behavior shown in Figure 5. Even though

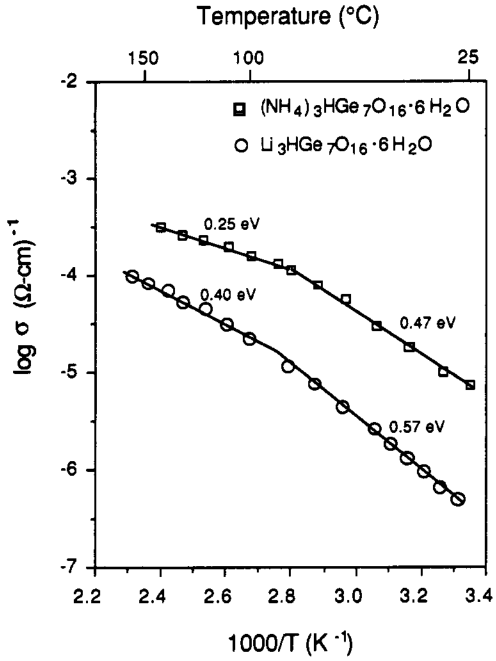

Figure 5. Temperature dependence of conductivity of hydrated $(NH_4)_3HGe_7O_{16}{\cdot}6H_2O$ and $Li_3HGe_7O_{16}{\cdot}6H_2O$.

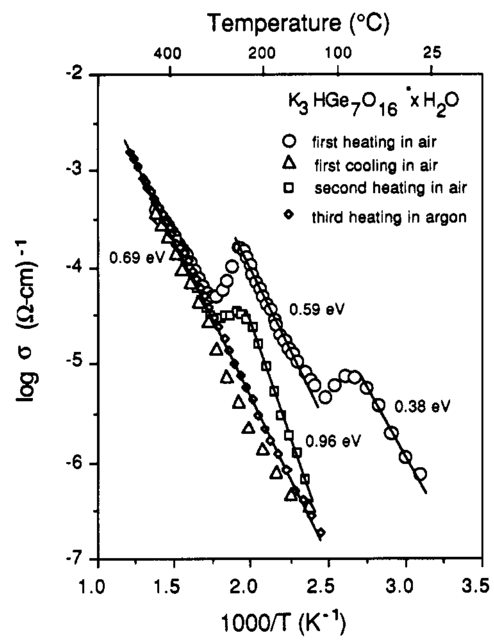

Figure 6. Temperature dependence of conductivity of hydrated $K_3HGe_7O_{16}{\cdot}xH_2O$ at different hydration levels.

$(NH_4)_3HGe_7O_{16}{\cdot}6H_2O$ loses more water than $Li_3HGe_7O_{16}{\cdot}6H_2O$ at the same temperature (as indicated by the TG curves in Figure 4), the ionic conductivity of the NH_4^+ sample is higher than that of the Li^+ form. Similarly, the activation energy for the NH_4^+ form is smaller than that in the Li^+ analogue. This is probably due to the formation of hydrogen-bonded chains of $H_2O{-}NH_4^+$ in the channels of $(NH_4)_3HGe_7O_{16}{\cdot}6H_2O$. Moreover, the NH_4^+ ion itself may be a source of protons. Conductivity was not observed in vacuum-dehydrated samples of $(NH_4)_3HGe_7O_{16}$ in this temperature range. The change in the slope of log σ vs $1/T$ plots in Figure 5 is ascribed to loss of water from the samples. The reason for the decrease in E_a above the critical temperature is not clear.

The conductivity behavior of a fully hydrated sample of $K_3HGe_7O_{16}{\cdot}4H_2O$, shown in Figure 6, is characterized by three unique regions, which suggest three different

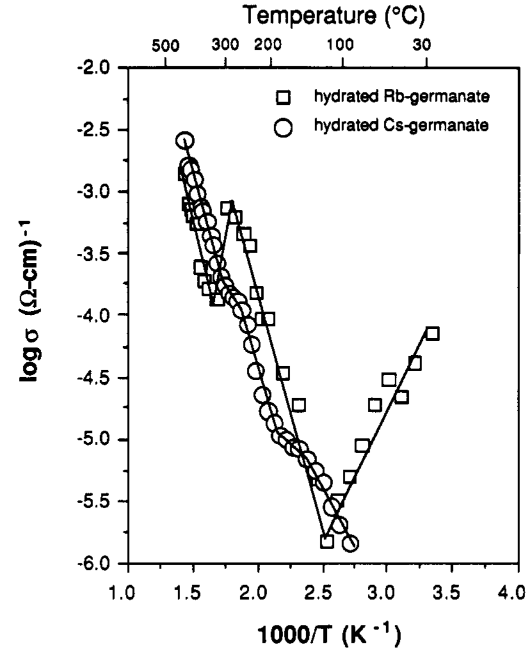

Figure 7. Conductivities of hydrated $Rb_3HGe_7O_{16}{\cdot}4H_2O$ and $Cs_3HGe_7O_{16}{\cdot}4H_2O$ as a function of temperature.

mechanisms of ion motion. From room temperature to 100 °C the conductivity increases with a relatively small E_a = 0.38 eV. The magnitude of E_a is in the range of "particle-like" or surface proton conductivity.[23] When the water, which facilities proton conductivity in this temperature range is lost, the conductivity decreases. The loss of one of the four H_2O molecules was also indicated by the TGA and DTA results (Figures 3 and 4) at ~100 °C. Thus it appears that below 100 °C this H_2O molecule is in a unique site in the structure and promotes fast proton conduction. Upon increasing the temperature ($T > 100$ °C), the conductivity increases again with E_a = 0.59 eV until ~275 °C and then decreases until ~300 °C. This region of the log σ vs $1/T$ plot is attributed to proton conductivity associated with the remaining water molecules. At 300 °C all of the water is lost from the sample to yield $K_3HGe_7O_{16}$. The increase in the conductivity from 300 °C to the decomposition temperature (680 °C) of this phase is ascribed to motion of K^+ ions with $E_a \sim 0.69$ eV.

This same sample of $K_3HGe_7O_{16}$ was first cooled to ~100 °C in air and was then heated in air to 400 °C (second heating cycle in Figure 6). It is noteworthy that the first cooling curve as well as the third heating curve in Ar(g) follow Arrhenius behavior and coincide with the conductivity curve of the first cycle in the $T > 275$ °C region, which was attributed to K^+ conductivity (i.e., there is no water in the sample at this temperature). However, the conductivities of the sample, in the region 100–275 °C, on second heating in air are higher than those in the first cooling in air and third heating in argon. As was indicated before, based on TGA cooling curves, $K_3HGe_7O_{16}$ contains ~1.5 mol of water at 100 °C. It can be seen (Figure 6) that the protonic conductivity of the sample with more water (i.e., first heating cycle; $x \sim 4$) is higher than that of the sample with less water (i.e., second heating cycle; $x \sim 1.5$) at the same temperature. Similarly, the activation energy for proton conduction in the more hydrated sample is lower than that for the less hydrated sample. These results clearly illustrate that the water content is a critical factor

(23) Barboux, P.; Morinean, R.; Livage, J. *Solid State Ionics* **1988**, *27*, 221.

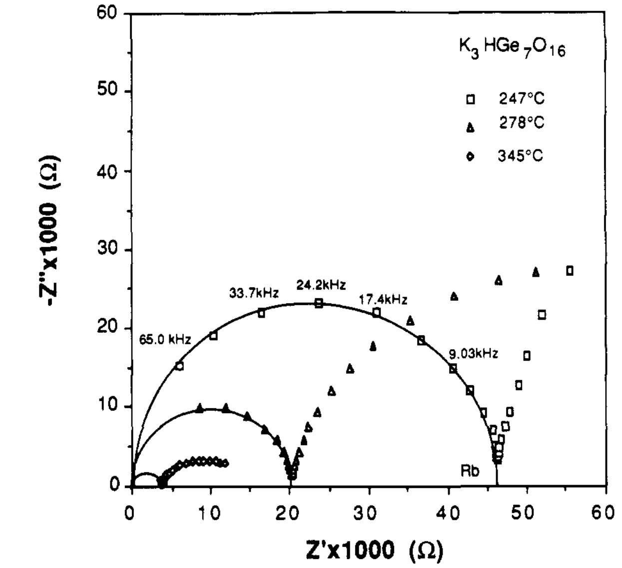

Figure 8. Ac impedance spectra for dehydrated $K_3HGe_7O_{16}$ at selected temperatures, 247, 278, and 345 °C; R_b is bulk resistance; solid line is drawn to guide the eye.

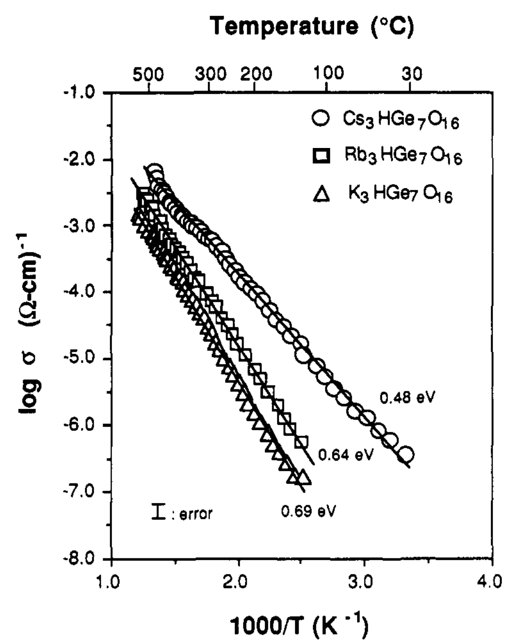

Figure 9. Temperature dependence of conductivity for dehydrated $M_3HGe_7O_{16}$, M = K^+, Rb^+, and Cs^+, in Ar gas.

for fast proton conductivity.

The conductivities of hydrated $Rb_3HGe_7O_{16}\cdot 4H_2O$ and $Cs_3HGe_7O_{16}\cdot 4H_2O$ as a function of temperature were also measured (Figure 7). The hydrated sample of the Rb analogue shows slightly higher conductivity than the dehydrated samples (Figures 9). The TGA curve for the Rb phase (Figure 4) shows that with increasing temperature, from 60 to 250 °C, water is lost from $Rb_3HGe_7O_{16}\cdot 4H_2O$ with a steady slope; even though, two endothermal peaks were observed in the DTA in this temperature region (Figure 3). In the Rb analogue, the variation of conductivity is consistent with the TGA data. The conductivity decreases from 30 to 145 °C probably due to loss of one type of water and then increases up to ~300 °C, which is probably because of the conductivity of another type of H_2O. Above 350 °C, in agreement with the TGA data (Figure 4), no more water remains in the sample. The increase in the conductivity above 350 °C is attributed to Rb^+ motion.

Table III. Selected Protonic Conductivities (σ) and Activation Energies (E_a) for Hydrated $M_3HGe_7O_{16}\cdot xH_2O$, M = NH_4^+, Li^+, and K^+

samples	temp, °C	σ, Ω cm^{-1}	E_a, eV
$(NH_4)_3HGe_7O_{16}\cdot xH_2O$	84	1.2×10^{-4}	0.25
	144	3.1×10^{-4}	
$Li_3HGe_7O_{16}\cdot xH_2O$	101	2.2×10^{-5}	0.40
	160	1.0×10^{-4}	
$K_3HGe_7O_{16}\cdot xH_2O$	162	1.1×10^{-5}	0.59
	245	1.6×10^{-4}	

The log σ vs 1/T behavior of the hydrated $Cs_3HGe_7O_{16}\cdot 4H_2O$ (Figure 7) is very different from that of the K and Rb analogues. No mechanism associated with proton conductivity is indicated (i.e., presence and loss of H_2O is not evident). The observed low conductivity in the hydrated sample (see Figure 9), compared to that in the dehydrated sample, is attributed to the restricted motion of Cs^+ ions when they are associated with water molecules $[Cs(H_2O)_x]^+$.

Selected protonic conductivities and activation energies for hydrated samples are listed in Table III. Although the mechanism of protonation in the hydrated alkali metal germanates is not clear, we have cited evidence that protons most likely form via the ionization of water molecules by cations:[21]

$$M(H_2O)_n^{m+} \rightarrow MOH(H_2O)_{n-1}^{(m-1)+} + H^+$$

This reaction is facilitated on the active intersurface of the channels, where the protons can migrate along the conducting path provided by water and/or ammonia molecules. The extent of proton formation (i.e., $M^+ + H_2O \rightarrow MOH + H^+$) decreases as the cation radius increases,[24] which is consistent with the magnitude of proton conductivity and activation energy; that is, the proton conductivity decreases from the hydrated Li form to the hydrated Cs form (almost no proton conductivity in the hydrated Cs form).

3.3.2. Dehydrated $M_3HGe_7O_{16}$, M = K^+, Rb^+, and Cs^+. To study pure M ionic conductivity, dehydrated samples of $M_3HGe_7O_{16}$ were used for the ac impedance measurements with identical experimental conditions maintained for each sample. Each as-prepared sample was preheated at 550 °C for 2 h (at this temperature water is fully removed from the channels as indicated by the TGA results (Figure 4)) and then cooled in dry flowing Ar gas to room temperature. The conductivity measurements were carried out in dry flowing Ar gas. Ac impedance data for $K_3HGe_7O_{16}$ at different temperatures are shown in Figure 8. Similar curves were also observed for $Rb_3HGe_7O_{16}$ and $Cs_3HGe_7O_{16}$. The observed semicircles passing through the origin are characteristic of bulk property. A simple equivalent circuit composed of the bulk resistance (R_b) in parallel with grain capacitance (C_g) is an adequate model of the equivalent circuit in the present systems. From the intercept of the semicircle with the Z' axis (the real part of impedance) in Figure 8, the overall resistance was determined.

The temperature dependence of conductivity (log σ vs $1/T$) of $M_3HGe_7O_{16}$, M = K^+, Rb^+, and Cs^+ is linear over the temperature range measured (Figure 9). The activation energies (E_a) were obtained from the Arrhenius plots, using the relationship $\sigma T = \sigma_0 e^{-E_a/RT}$. In general, E_a is comprised of the energy term necessary to generate defect sites in the crystal, E_f, and the energy needed for the ions to overcome potential barriers during migration, E_m. For microporous

(24) Sposito, G. *The Surface Chemistry of Soils*; Oxford University Press: New York, 1984; p 69.

Table IV. Typical Ionic Conductivities and Activation Energies of Dehydrated $M_3HGe_7O_{16}$, M = K^+, Rb^+, and Cs^+

sample	ionic conductivity, $(\Omega\ cm)^{-1}$ 200 °C	300 °C	400 °C	500 °C	E_a, eV
$K_3HGe_7O_{16}$	1.8×10^{-6}	3.3×10^{-5}	2.3×10^{-4}	8.7×10^{-4}	0.69
$Rb_3HGe_7O_{16}$	7.2×10^{-6}	9.3×10^{-5}	5.0×10^{-4}	2.1×10^{-3}	0.64
$Cs_3HGe_7O_{16}$	1.1×10^{-4}	6.8×10^{-4}	2.0×10^{-3}	8.9×10^{-3}	0.48

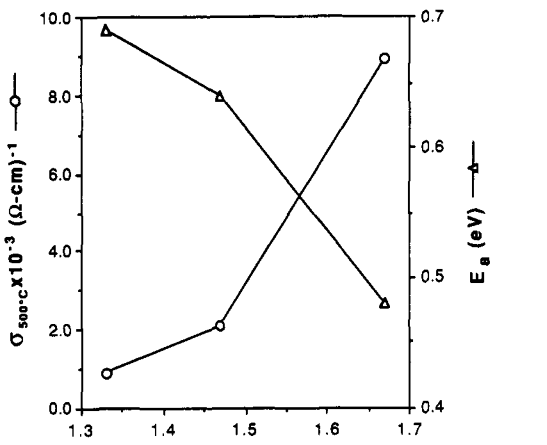

Figure 10. Relationship of ionic conductivity, σ, at 500 °C and activation energy, E_a, with cation radius (r).

materials the number of thermally generated defect sites is generally small in comparison with the number of existing structural empty sites. Therefore, the activation energy obtained is dominated by the value of the potential barrier, E_m. The activation energies of conductivities for $M_3HGe_7O_{16}$, M = K^+, Rb^+, and Cs^+, are 0.69 (K), 0.64 (Rb), and 0.48 eV (Cs). The decreasing activation energy with increasing cationic radius is expected because the Coulombic attraction between the cations and the negatively charged framework structure decreases with increasing cation radius (K^+, 1.33; Rb^+, 1.47; Cs^+, 1.67 Å). The ionic conductivities at different temperatures and the activation energies are listed in Table IV. It is interesting to compare the values of activation energies for $M_3HGe_7O_{16}$ with those of the highest conducting zeolites with K^+, Rb^+, and Cs^+ cations. The E_a values obtained for $M_3HGe_7O_{16}$ are much lower than those for K, Rb, and Cs analcime (0.76, 0.73, and 0.94 eV, respectively) and for K and Rb sodalite (0.96 and 0.94 eV, respectively)[7] whose framework structures contain only two-coordinate oxygens. The best ionic conductivity, 2.0×10^{-3} $(\Omega\ cm)^{-1}$ at 400 °C in $Cs_3HGe_7O_{16}$, is significantly higher, at comparable temperatures, than those reported in zeolites to date. Moreover, the room-temperature conductivity of $Cs_3HGe_7O_{16}$, $\sim 10^{-6}$ $(\Omega\ cm)^{-1}$, is quite high.

Correlation between cation size, activation energy (E_a), and ionic conductivity (σ) is shown in Figure 10. As the cation radius increases, the activation energy decreases and the conductivity increases. This behavior is due to the decrease of the effective charge of the cation (Z/r) with increasing cation radius (r), which results in a relatively weaker interaction between the negatively charged framework structure of the zeolite with the larger cations.

For $(NH_4)_3HGe_7O_{16}{\cdot}6H_2O$ and $Li_3HGe_7O_{16}{\cdot}6H_2O$, as mentioned above, the decomposition temperatures are at about 170 and 260 °C, respectively. However, even close to the decomposition temperature some water is retained in the structure (i.e., TGA data, Figure 4), which implies that for structures with small cations, the water molecules may play an important role as structure templates. Above 260 °C $Li_3HGe_7O_{16}{\cdot}6H_2O$ becomes amorphous; at 560 °C

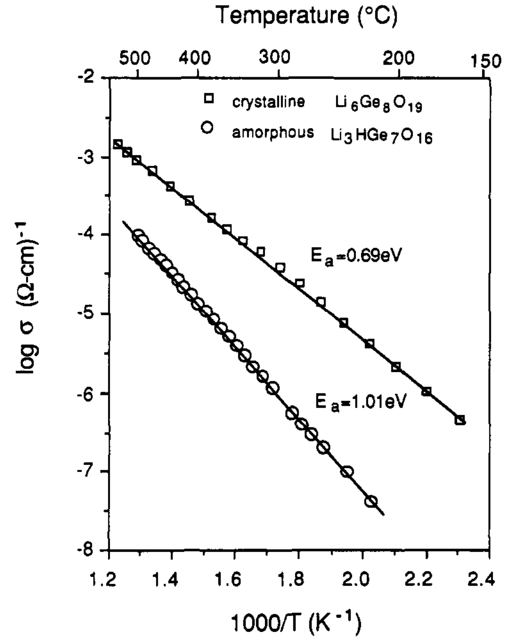

Figure 11. Temperature dependence of conductivity of $Li_6Ge_8O_{19}$ and $Li_3HGe_7O_{16}$.

this amorphous phase crystallizes to a lithium germanate, $Li_6Ge_8O_{19}$, which is stable up to 953 °C.[25] Figure 11 shows the ionic conductivity of both amorphous $Li_3HGe_7O_{16}$ and its decomposition product, mostly crystalline $Li_6Ge_8O_{19}$. This phase is actually a composite of primarily crystalline $Li_6Ge_8O_{19}$ and amorphous GeO_2 (see section 3.2.2). The ionic conductivity of the amorphous $Li_3HGe_7O_{16}$ is lower ($\sigma_{500°C} \sim 1.0 \times 10^{-4}$ $(\Omega\ cm)^{-1}$ and E_a is higher ($E_a \sim 1.01$ eV) than that of the crystalline $Li_6Ge_8O_{19}$ phase ($\sigma_{500°C} \sim 1.0 \times 10^{-3}$ $(\Omega\ cm)^{-1}$ and $E_a \sim 0.69$ eV).

4. Conclusions

In summary, a series of novel crystalline, microporous germanates, $M_3HGe_7O_{16}{\cdot}xH_2O$, M = NH_4^+, Li^+, K^+, Rb^+, and Cs^+, were synthesized from hydrothermal systems and characterized by X-ray diffraction and thermal analyses. Proton and cation conductivities were observed in hydrated and dehydrated samples, respectively. For the hydrated samples, the extent of ionization of water molecules (protonation) by the cations and the water and/or ammonia content (formation of conducting path) dramatically effect the magnitude of proton conductivity. The activation energies for ion conduction in dehydrated $M_3HGe_7O_{16}$, M = K^+, Rb^+, and Cs^+, are 0.69, 0.64, and 0.48 eV, respectively. The decreasing activation energy with increasing cationic radius was attributed to the decrease of the Coulombic attraction between the cations and the negatively charged framework structure. The highest ionic conductivity, 2.0×10^{-3} $\Omega\ cm^{-1}$ at 400 °C, was found in $Cs_3HGe_7O_{16}$; and the protonic conductivity, 3.1×10^{-4} $\Omega\ cm^{-1}$ is observed at 144 °C in $(NH_4)_3HGe_7O_{16}{\cdot}6H_2O$. Compared with aluminosilicate zeolites, the germanates studied here show higher ionic conductivities and lower activation energies. It was concluded that in the germanates the electrostatic interaction between the mixed GeO_4 and GeO_6 anion framework structure and the cations in the channels is less than that between the tetrahedral anionic network of zeolites and their cations. A matching of the size of the mobile cations and the channel dimensions of the zeolite-like structures is important to promote

(25) Murthy, M. K.; Ip, J. *J. Am. Ceram. Soc.* **1960**, *47*, 328.

ionic conductivity in microporous structures.

Acknowledgment. We wish to thank Dr. M. Tsai for valuable discussion in ionic conductivities and Prof. W. McCarroll for his helpful comments. This is publication No. D10550-6-91 of the New Jersey Agricultural Experiment Station supported by State Funds and the Center for Advanced Food Technology (CAFT). The Center for Advanced Food Technology is a New Jersey Commission on Science and Technology Center.

Registry No. $(NH_4)_3HGe_7O_{16}\cdot 6H_2O$, 139311-81-2; $Li_3HGe_7O_{16}\cdot 6H_2O$, 139311-80-1; $K_3HGe_7O_{16}\cdot 4H_2O$, 12395-61-8; $Rb_3HGe_7O_{16}\cdot 4H_2O$, 12529-64-5; $Cs_3HGe_7O_{16}\cdot 4H_2O$, 139311-82-3; $K_3HGe_7O_{16}$, 12195-29-8; $Rb_3HGe_7O_{16}$, 12195-32-3; $Cs_3HGe_7O_{16}$, 12191-09-2; $Li_6Ge_8O_{19}$, 51912-96-0; $Li_3HGe_7O_{16}$, 12195-30-1.

Preparation, Characterization, and Ionic Conductivity of Novel Crystalline, Microporous Silicogermanates, $M_3HGe_{7-m}Si_mO_{16}\cdot xH_2O$, M = K^+, Rb^+, Cs^+; $0 < m < 3$; x = 0–4. 3

Shouhua Feng, Menting Tsai, Sung-Ping Szu, and Martha Greenblatt*

Department of Chemistry, Rutgers, The State University of New Jersey, Piscataway, New Jersey 08855-0939

Received November 20, 1991. Revised Manuscript Received January 14, 1992

Crystalline, microporous silicogermanates, $M_3HGe_{7-m}Si_mO_{16}\cdot xH_2O$, M = K^+, Rb^+, and Cs^+, $0 < m < 3$, x = 0–4, were synthesized from hydrothermal systems and characterized by powder X-ray diffraction, differential thermal and thermogravimetric analysis, Fourier transform infrared, and solid-state ^{29}Si nuclear magnetic resonance techniques. Ionic conductivity in dehydrated samples was investigated by ac impedance in the temperature range 25–550 °C. The framework substitution of Si for Ge at tetrahedral positions leads to a significant increase of ionic conductivity and decrease of activation energy. The effects of the silicon content and size of ionic radius on the activation energy and ionic conductivity are discussed.

1. Introduction

In previously reported work[1,2] on the preparation and ionic conductivity of a series of crystalline, microporous germanates, $M_3HGe_7O_{16}\cdot xH_2O$, M = Li^+, NH_4^+, Na^+, K^+, Rb^+, and Cs^+, we found that the dehydrated samples have better ionic conductivity than the traditional zeolites. The cubic framework structure of the germanates is built up of face- and edge-sharing GeO_6 octahedra which corner share with GeO_4 tetrahedra (Figure 1). There are three four-coordinated and four six-coordinated Ge atoms in the unit cell. Four out of sixteen framework oxygen atoms are four-coordinated by Ge atoms and a hydrogen atom, which is located in the center of the cell.[3] There are channels of eight-membered rings with a window size of ~4.3 Å in the [100] direction that contain the mobile cations and water molecules. It was shown that these materials with mixed GeO_4–GeO_6 polyhedra forming a framework structure have potential applications as molecular sieves, ion-conducting electrolytes, and humidity sensing materials. However, compared with typical fast ion conductors,[4,5] the activation energy for ionic conduction in these materials is higher, which lowers the ionic conductivity in the low temperature range. In this present work, we attempt to improve the conductivity in the germanates via substitution of SiO_4 for GeO_4. The substitution of Si^{4+} for Ge^{4+} is expected to weaken the electrostatic interaction between mobile cations and the framework oxygens because the Si–O bond is more covalent, which polarizes the oxygen charge density more strongly toward the Si atoms so as to give the framework oxide ions a lower effective negative charge.

Here we report the results of the hydrothermal crystallization, structural characterization, and ionic conductivity of $M_3HGe_{7-m}Si_mO_{16}\cdot xH_2O$, M = K^+, Rb^+, and Cs^+, $0 < m < 3$.

2. Experimental Section

$M_3HGe_{7-m}Si_mO_{16}\cdot xH_2O$, M = K^+, Rb^+, and Cs^+ were directly synthesized hydrothermally at 180–200 °C in sealed systems containing an aqueous mixture of MOH, the α-quartz form of germanium dioxide, and SiO_2 sol. A typical synthesis began with the combination of GeO_2 (Eagle-Picher Co., reagent grade) and the aqueous solution of alkali metal hydroxide (KOH, RbOH, or CsOH, Fisher, reagent grade) to form an aqueous solution; SiO_2 sol (AESAR, Johnson Matthey INC) was added to the first solution. Crystallization of the aqueous gel was carried out in stainless steel autoclaves lined with poly(tetrafluoroethylene) (PTFE) under autogenous pressure at empirically determined temperatures. The crystalline product was filtered, washed with distilled water and dried at ambient temperature.

The powder X-ray diffraction (XRD) patterns were recorded on a Scintag X-ray diffractometer with monochromatized Cu $K\alpha$ radiation. Unit-cell parameters were obtained with a least-squares method, with silicon as an internal standard. The analysis of Si content was carried out on a Beckman Spectrometric Spectraspan IIIB DCT Basic Multi dc argon plasma emission spectrometer. Differential thermal analysis (DTA) and thermogravimetric analysis (TGA) were carried out on a Du Pont Model 9900 thermal analyzer with a heating rate of 10 °C/min in air. Fourier transform infrared (FTIR) spectra were recorded at room temperature on

* To whom correspondence should be addressed.

(1) Feng, S.; Tsai, M.; Greenblatt, M. *Chem. Mater.*, in press.
(2) Feng, S.; Greenblatt, M. *Chem. Mater.*, previous paper in this issue.
(3) Nowotny, H.; Wittmann, A. *Monatsh. Chem.* **1954**, *85*, 561.
(4) Goodenough, J. B.; Hong, H. Y.-P.; Kafalas, J. A. *Mater. Res. Bul.* **1976**, *11*, 203.
(5) Hong, H. Y.-P. *Mater. Res. Bul.* **1978**, *13*, 117.

0897-4756/92/2804-0468$03.00/0